

# Optical Intensity Interferometry through Atmospheric Turbulence

P. K. Tan<sup>1,2\*</sup>, A. H. Chan<sup>2</sup>, and C. Kurtsiefer<sup>1,2</sup>

<sup>1</sup>Centre for Quantum Technologies, 3 Science Drive 2, 117543, Singapore

<sup>2</sup>Department of Physics, National University of Singapore, 2 Science Drive 3, 117551, Singapore

## ABSTRACT

Conventional ground-based astronomical observations suffer from image distortion due to atmospheric turbulence. This can be minimized by choosing suitable geographic locations or adaptive optical techniques, and avoided altogether by using orbital platforms outside the atmosphere. One of the promises of optical intensity interferometry is its independence from atmospherically induced phase fluctuations. By performing narrowband spectral filtering on sunlight and conducting temporal intensity interferometry using actively quenched avalanche photon detectors (APDs), the Solar  $g^{(2)}(\tau)$  signature was directly measured. We observe an averaged photon bunching signal of  $g^{(2)}(\tau) = 1.693 \pm 0.003$  from the Sun, consistently throughout the day despite fluctuating weather conditions, cloud cover and elevation angle. This demonstrates the robustness of the intensity interferometry technique against atmospheric turbulence and opto-mechanical instabilities, and the feasibility to implement measurement schemes with both large baselines and long integration times.

**Key words:** atmospheric effects – radiation mechanisms: thermal – techniques: interferometric

## 1 OPTICAL INTENSITY INTERFEROMETRY

Hanbury-Brown & Twiss (1954, 1956) demonstrated that at sufficiently short baselines or timescales, both the spatial and temporal correlation measurements of thermal light sources such as the stars should exhibit a photon bunching signal, which was later generalised by Glauber (1963) as the second order correlation,  $g^{(2)}$ , that peaks at twice the value of the statistically random noise floor:

$$g^{(2)}(\tau, b) = 1 + e^{-2|\tau|/\tau_c} |\gamma(b, l_c)|^2, \quad (1)$$

where  $\tau$  is the detection time difference,  $\tau_c$  the coherence time of a light source with a Lorentzian spectral profile, and  $\gamma$  a (complex) spatial coherence function depending on the spatial separation  $b$  of the two detectors and an effective spatial coherence length  $l_c$  of the light source. This correlation signature is independent of the optical phase, and forms the basis for intensity interferometry, which has the benefit of being insensitive to first order noise contribution from urban light pollution and atmospheric turbulence (Davis et al. 1999).

The spatial correlation  $g^{(2)}(\tau = 0, b)$  imparts information about the shape and intensity distribution of the light source, while the temporal correlation  $g^{(2)}(\tau, b = 0)$  reveals the characteristic emission mechanism of its source, such

as whether its a coherent laser light or an incoherent thermal source (Morgan & Mandel 1966; Mandel & Wolf 1995; Loudon 2000; Saleh & Teich 2007).

Intensity interferometric measurements revealing information about the angular size via  $l_c$  (Hanbury-Brown 1974), and the emission nature of the light source via  $t_c$  are so in turn potentially affected by decoherence in the spatial and temporal domains, respectively. It is therefore important to investigate the influence of atmospheric effects on intensity correlation measurement of celestial objects.

### 1.1 Atmospheric Turbulence

Atmospheric turbulence introduces scintillation with a characteristic timescale on the order of microseconds, and a spatial inner scale of approximately 3 mm for typical wind speeds of  $10 \text{ ms}^{-1}$  (Dravins et al. 1997), corresponding to delay time variations on the order of tens of picoseconds due to fluctuations in the atmospheric path difference (Dravins & LeBohec 2007; Cavazzani et al. 2012). This sets the lower bound on effective detector timing resolution to be in the 10 ps regime before it is constrained by the atmospheric scintillation. This timing uncertainty due to the varying refractive index in the atmospheric layers (Marini & Murray 1973) has been observed in laser ranging experiments (Kral et al. 2004; Blazej et al. 2008). The Wiener-Khinchin theorem asserts that the auto-correlation

\* pengkian@physics.org

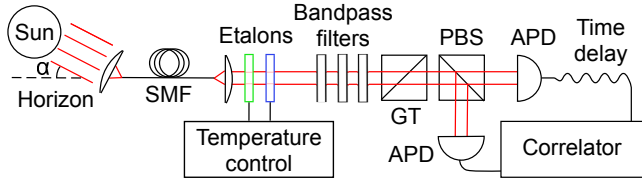


**Figure 1.** Optical setup. Sunlight is coupled into a single mode optical fibre for spatial mode filtering, and then exposed to a stack of spectral filters, consisting of two temperature-stabilised etalons E1, E2, and a bandpass filter stack (BPF) of three interference filters. One polarisation of the transmitted narrow spectrum is selected with a Glan-Taylor polariser, and distributed with a polarising beam splitter (PBS) onto two avalanche photodiodes (APD) for photo-detection time analysis.

function of a stationary random process is given by the Fourier transform of its power spectrum, which may pick up this timing uncertainty.

The most commonly considered influence of the atmosphere on astronomical observations is the seeing, which extends the diffraction-limited Airy patterns of stellar light sources into seeing discs, with a typical diameter on the order of arcseconds.

Of more concern for observation of temporal correlations are chromatic dispersion effects which can be suppressed by operating in a narrow optical bandwidth. The atmosphere also induces phase difference of about 0.5 radian between optical light waves with a frequency difference of only a few Gigahertz (GHz) (Dravins et al. 2005), and a corresponding loss of correlation estimated to be less than 1%. This suggests a practical spectral bandwidth in the range of GHz to suppress this chromatic dispersion.

In this work, we investigate the influence of turbulence in an atmospheric column varying over the time of the day on the photon bunching signature in an intensity correlation measurement, and therefore the effective length of the air column. The optical bandwidth in our experiment is narrow enough to resolve the temporal correlation  $g^{(2)}(\tau)$  to assess the emission nature of a light source, and eventually detect decoherence effects of non-atmospheric origin.

## 2 EXPERIMENTAL SETUP

Similar to our earlier work (Tan et al. 2014), sunlight is collected by an aspheric lens with an effective focal length of 4.51 mm into a single mode optical fibre (Thorlabs 460HP, single mode for 450–600 nm, numerical aperture NA = 0.13), resulting in an effective lens aperture of 1.2 mm. The small diameter aspheric lens is sufficient here because the Sun is an angularly extended thermal light source. Thus, the number of photons per spatial mode per unit frequency distribution is defined only by the source surface temperature, and independent of the collection aperture size (Stokes 1994).

The projection into the fundamental TEM<sub>00</sub> Gaussian mode of the single mode fibre leads to a light field with perfect spatial coherence behind the optical fibre, which is then directed through an arrangement of narrowband spectral filtering as illustrated in Fig. 1.

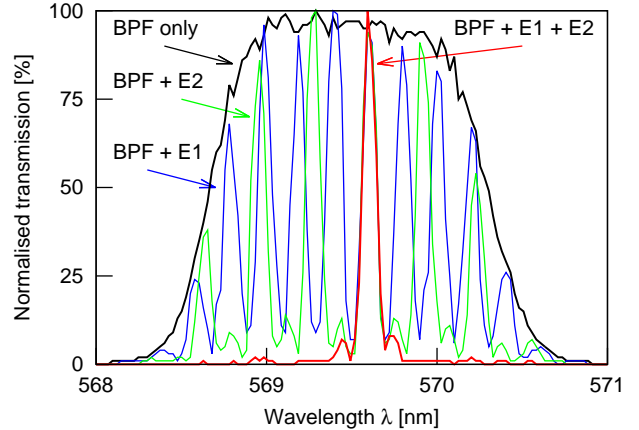


**Figure 2.** Transmission profile of the filter stack. The black trace shows the bandpass filter stack (BPF) only, with a width of 2 nm (FWHM). When adding etalon E1 (thickness 0.5 mm), several transmission peaks fall into the window selected by the BPF. Similarly, wider spaced transmission peaks are visible with etalon E2 (thickness 0.3 mm). When combining both etalons and the BPF, only one transmission peak is left, with small residual contributions about 0.6 nm due to near-overlaps. The line width of the transmission peaks with the etalons is dominated by the spectrometer response of 0.12 nm, the actual line width should be around 0.002 nm.

### 2.1 Filter stack

In the filtering scheme reported here, Sunlight leaving the optical fibre is collimated by an aspheric lens with an effective focal length of 4.6 mm. The light is then sent through two plane-parallel solid etalons made out of fused silica (Suprasil311) of thickness 0.5 mm and 0.3 mm, respectively. With a refractive index of  $n = 1.460$  around 546–570 nm, this corresponds to a free spectral range

$$FSR = \frac{c}{2dn} \quad (2)$$

of approximately 205 GHz and 342 GHz, respectively. The etalons have reflective coatings of  $R = 97\%$  at 546.1 nm on both sides. Neglecting losses in the coatings, the finesse (Fox 2006)

$$\mathcal{F}_R = \frac{\pi\sqrt{R}}{1-R} = 103 \quad (3)$$

of the etalons leads to a transmission bandwidth of  $\Delta f_{FWHM} = FSR/\mathcal{F}_R = 3.32$  GHz for the 0.3 mm etalon, and  $\Delta f_{FWHM} = 1.99$  GHz for the 0.5 mm etalon, respectively. The spectral transmission profiles of the etalons are tuned via temperature, with a tuning coefficient of  $-4.1$  GHz/K. Temperature tuning was used in lieu of physical rotation of the etalons to avoid ‘walk-off’ effects (Green 1980), and for mechanical stability of the setup.

A series of three interference bandpass filters are used to reject all other wavelengths: two narrowband filters of central wavelength (CWL) = 569.6 nm with Full Width at Half Maximum (FWHM) of 2.2 nm and a broadband filter with CWL = 540 nm and FWHM = 80 nm. The transmission profile of the bandpass filters (BPF), and the transmission profiles of a combination of the BPF with etalons is shown in Fig. 2. For a single etalon, several transmission peaks corresponding to its free spectral range fall into the

transmission window of the BPF. By combining both etalons with their different free spectral ranges, we can achieve single transmission peak in the BPF window, and thus a single transmission window over the whole optical frequency range. The transmission profiles shown for the etalons are wider than actual due to the spectrometer resolution limited at 0.12 nm. This corresponds to a bandwidth of about 110 GHz, so we are unable to resolve the transmission bandwidth of the etalons. Equally, the side lobes next to the transmission peak in Fig. 2 are an artefact of the spectrometer we used. We estimate the peak transmission of the etalon and filter stack to be around 84%, improving the transmission of the grating/etalon stack in our earlier work (Tan et al. 2014) by about a factor of 4.

The strong emission line at 569.6 nm in Gamma Velorum ( $\gamma$  Vel), which is the brightest Wolf-Rayet star at visual apparent magnitude  $m_v = 1.7$ , is a prime natural laser source candidate (Dravins & Germanà 2008), and would be an interesting light source to apply this photon correlation method to. Therefore, this wavelength was chosen as an instrumental proof-of-concept. To centre the peak transmission of the etalon stack at 569.6 nm, we filtered the blackbody spectrum of an Argon arc lamp with a grating monochromator to a bandwidth of about 0.12 nm. With this, we could align the bandpass interference filters, and tune the etalon temperatures. The 0.5 mm etalon had to be maintained at 59.2°C, and the 0.3 mm etalon at 64.0°C.

## 2.2 Intensity correlation scheme

A Glan-Taylor polariser (GT) selects linearly polarised light to optimise spatial mode correlations and in conjunction with a polarising beamsplitter (PBS) and allows to balance the individual detector count rates, thus minimising the measurement duration. This configuration also helps to suppress cross-talk coincidence events arising from the APD breakdown flash (Kurtsiefer et al. 2001).

Finally, the light is detected by two actively quenched Silicon Avalanche Photon Detectors (APDs). An oscilloscope with a sampling rate of 40 GS/s was used to determine the temporal correlation  $g^{(2)}(\tau)$ . The combined effective timing jitter of photodetectors and oscilloscope was measured to be around  $\tau_j = 40$  ps (FWHM), but the timing response of the two photodetectors (taken with a correlated photon pair source based on parametric down conversion (Ling et al. 2008), generating photon pairs around 810 nm within a time of about 0.7 ps, much shorter than the time constants of the photodetectors) has a peculiar structure (see Fig. 3). The coincidence distribution of the detectors shows a narrow peak leading to the small full width at half maximum, but a relatively large base that seems to reflect an exponential decay. The solid line in the figure represents a heuristic model

$$G^{(2)}(\tau) = A \frac{1}{\sqrt{2\pi\sigma^2}} e^{-\tau^2/2\sigma^2} + B \frac{1}{\tau_e} e^{-2|\tau|/\tau_e}, \quad (4)$$

with a time constant  $\sigma = 12.0 \pm 0.1$  ps for the Gaussian, and  $\tau_e = 450 \pm 2$  ps for the exponential decay for a fit over the time window  $\tau = -1 \dots 1$  ns. The weight  $A$  and  $B$  of the two distributions is about the same. We don't have a precise model of the photodetector, but note that this detector

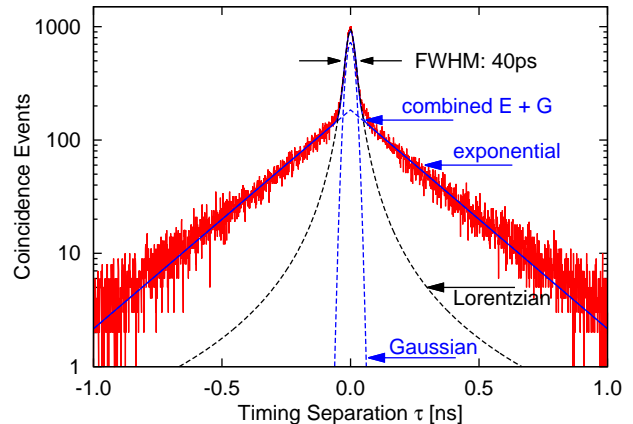


**Figure 3.** Photodetection coincidence histogram from photon pairs at a wavelength of 810 nm generated by parametric down conversion. These photon pairs have an intrinsic timing spread of about 0.7 ps, so this coincidence histogram reveals information about the timing uncertainty introduced by the detection mechanism only, dominated by the APD timing jitter. The dominant central structure can be fitted to a Gaussian, with long tails following an exponential decay.

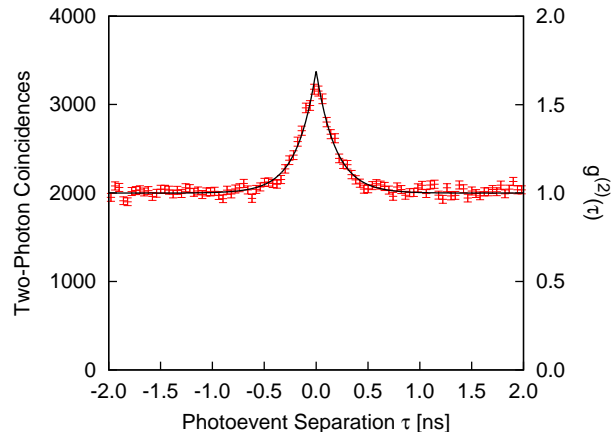


**Figure 4.** Raw coincidence histogram and normalised intensity correlation function  $g^{(2)}(\tau)$  for the Sun, measured in a 4 minute interval at starting 11:36 am. The characteristic photon bunching signature decays exponentially with a time constant of  $\tau_e = 375 \pm 35$  ps from the maximum  $g^{(2)}(0) = 1.69 \pm 0.05$ .

response is most likely what limits the maximally observed photon bunching signature.

## 3 RESULTS

A typical measurement of the temporal correlation function  $g^{(2)}(\tau)$  of the Sun is shown in Fig. 4. The two-photon coincidence events are fitted to a distribution

$$g^{(2)}(\tau) = 1 + ae^{-2|\tau|/\tau_e}, \quad (5)$$

assuming a Lorentzian transmission profile of the etalon stack defining the frequency distribution, and allowing for a limited interferometric visibility  $V = g^{(2)}(0)/2 = (1 + a)/2$ . The fitted parameters give a peak value  $g^{(2)}(\tau = 0) =$

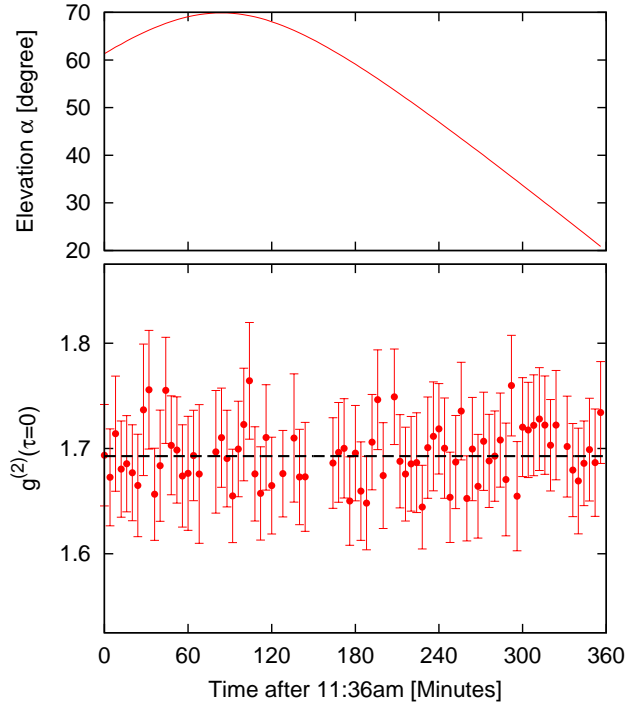


**Figure 5.** Bottom trace: Normalised peak correlation  $g^{(2)}(0)$  of the Sun, taken in 4 minute intervals over an extended duration from 11:36 am onwards. Top trace: the corresponding elevation  $\alpha$  of the Sun.

$1.69 \pm 0.05$  corresponding to an interferometric visibility  $V \approx 85\%$ , and a coherence time of  $\tau_c = 375 \pm 35$  ps.

The observed ratio of the photon bunching excess ( $g^{(2)} - 1$ ) to the noise given by the standard deviation  $\Delta$  evaluated from propagated Poissonian statistics in our experiment is  $\text{SNR} = (g^{(2)} - 1)/\Delta = 13.8$ . This is slightly smaller than the signal-to-noise ratio predicted in (Hanbury-Brown 1974),

$$\text{SNR} = \frac{1}{2} r_s \sqrt{\tau_j T} \approx 21, \quad (6)$$

where  $r_s \approx 300000 \text{ s}^{-1}$  is the counting rate on a single detector,  $\tau_j$  the time bin width for the pair histogramming (40 ps), and  $T = 4$  minutes the integration time for one measurement. The discrepancy could be explained by a varying  $r_s$  due to fast weather condition changes over  $T$ .

The measurements were conducted in the National University of Singapore observatory site, with geographical coordinates of  $1^\circ 17' 49'' \text{ N}$  and  $103^\circ 46' 44'' \text{ E}$ , on the 28th of May 2015, from 11:36 am to 5:36 pm (GMT +8:00), through varying cloud cover, weather conditions and elevation angular position of the Sun. In Fig. 5, the Solar  $g^{(2)}(\tau = 0)$  is shown for consecutive integration intervals  $T$  of 4 minutes. The corresponding elevation angle  $\alpha$  of the Sun given by

$$\sin(\alpha - R) = \sin \phi \sin \delta + \cos \phi \cos \delta \cos \omega \quad (7)$$

is shown in the top part of the figure, with latitude  $\phi$ , declination  $\delta$  and hour angle  $\omega$  (Woolf 1968) and a small heuristic correction  $R$  of at most 34 arc minutes due to the refraction in the atmosphere (Bennett 1982).

Over that measurement time where weather and building geometry permitted to collect data, the elevation angle  $\alpha$  covers a range from about  $70^\circ$  around noon to  $20^\circ$  in the

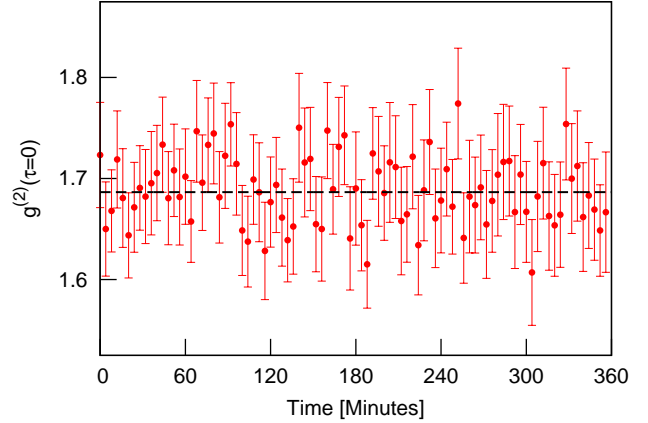


**Figure 6.** Normalised peak correlation  $g^{(2)}(0)$  of an Argon arc lamp in steps of 4 minutes for testing the thermal/temporal stability of the optical setup.

evening, making the length of the air column  $s = h_0 / \sin \alpha$  the light has to pass through to range from  $1.06h_0$  to  $2.92h_0$ , where  $h_0$  is the effective height of the atmosphere. Within the statistical uncertainty, we cannot see any change of the peak correlation  $g^{(2)}(\tau = 0)$ .

As reference, to investigate for decoherence effects by the atmospheric turbulence, we compare the observed Solar temporal correlation function with one obtained from light of an Argon arc lamp having a blackbody temperature of 6000 K and thus a suitable analogue to the Sun (see Figure 6), using exactly the same filter configuration as for the Sun. Both the Sun and the lamp lead to  $\approx 10^5$  photoevents per second to the APDs after the filtering scheme. For light from the Arc lamp, we find  $g^{(2)}(0) = 1.687 \pm 0.004$ .

The Solar measurement is compatible with a reference measurement performed with light from an arc lamp. This agreement suggests that atmospheric turbulence does not degrade the measurable visibility of temporal intensity interferometry, under our measurement scheme of 2 GHz optical bandwidth and 25 GHz electronic bandwidth.

The mean Solar  $g^{(2)}(0) = 1.693 \pm 0.003$  is significantly higher than our previous value of  $1.37 \pm 0.03$  (Tan et al. 2014), most likely due to the better off-resonance extinction of the etalon stack, combined with the two interference filters. The observed distribution  $\tilde{g}^{(2)}(\tau)$  from the filtered Sunlight should be determined by a convolution of the detector pair response  $D(\tau)$  with the idea correlation function  $g^{(2)}$  from (5),

$$\tilde{g}^{(2)}(\tau) = g^{(2)}(\tau) \otimes D(\tau) = \int g^{(2)}(\tau - \tau') D(\tau') d\tau'. \quad (8)$$

However, a direct convolution with the normalized measured detector contribution  $G^{(2)}$  shown in Figure 3,

$$D(\tau) = G^{(2)}(\tau) / \int G^{(2)}(\tau') d\tau', \quad (9)$$

significantly underestimates the observed  $\tilde{g}^{(2)}(0)$ , and leads to a much larger time constant  $\tau_c$  for the exponential decay in (5). We suspect that the fraction of photodetection events with a long decay time  $\tau_c$  seen in Figure 3 depends on the wavelength of the light (Ghioni et al. 2008), so a direct application to behaviour at the target wavelength of 569.6 nm



may not be justified. By using a Lorentzian distribution with the observed FWHM of  $\tau_j = 40$  ps,

$$D(\tau) = \frac{1}{\pi} \frac{\tau_j/2}{\tau_j^2/4 + \tau^2} \quad (10)$$

as shown in the dashed line in Figure 3, effectively ignoring the long decay fraction, we obtain a peak value of  $g^{(2)}(0) = 1.8$ , slightly overestimating the observed distribution. The remaining discrepancy could be due the deviation of the photodetector response  $D(\tau)$  from a Lorentzian, but also due to minor temperature inhomogeneities in the etalons, or a difference of the etalon line width due to operating it away from the etalon design wavelength of 546.1 nm.

#### 4 DISCUSSION AND APPLICATIONS

There has been a growing interest in recent years to revive the Hanbury-Brown–Twiss method (Ofir & Ribak 2006; Millour 2008; Foellmi 2009; Borra 2013; Dravins et al. 2015), which has the potential to map the spatial structure of stellar formations (Millour 2010; Dravins et al. 2013), detect exoplanets (Hyland 2005; Strekalov et al. 2013) and for kilometeric baseline arrays to achieve micro-arcsecond resolution (Barbieri et al. 2009; Borra 2013; Capraro et al. 2009; Dravins 2007; LeBohec et al. 2008; Nuñez 2012).

Our results suggest no significant decoherence to temporal photon bunching measurements, thus supporting such proposals. In particular, this measurement scheme provides for the possibility of temporal coherence studies, which might be useful in characterising natural laser candidates such as Eta Carinae or Wolf-Rayet stars (Castor & Nussbaumer 1972; van der Hucht 2001; Johansson & Letokhov 2005; Varshni & Nasser 1986; Roche et al. 2012), or preliminary probes into testing quantum gravity models (Milburn 1991, 2006; Lieu & Hillman 2003; Ng et al. 2003; Ragazzoni et al. 2003; Maziashvili 2009; Perlman et al. 2015). However, any such decoherence effects would be weak: a signature of such effects would be a small deviation from the photon bunching signature with  $g^{(2)}(\tau = 0) = 2$  of a thermal light source. For this, the current peak value of  $g^{(2)}$  is probably still too low, limited by the temporal resolution of the avalanche photodiodes.

However, with the resolution we have at hand, the Solar  $g^{(2)}(\tau)$  measurements demonstrate its robustness against atmospheric turbulence, affirming intensity interferometry as a serious consideration for both extensive baselines and protracted integration time measurements.

#### ACKNOWLEDGEMENTS

We acknowledge the support of this work by the National Research Foundation & Ministry of Education in Singapore.

#### REFERENCES

Barbieri C., et al., 2009, *Astro2010: The Astronomy and Astrophysics Decadal Survey*, 2010  
 Bennett G. G., 1982, *Journal of Navigation*, 35, 255  
 Blazej J., Prochazka I., Kral L., 2008, *Proc. SPIE*, 7152, 71520R  
 Borra E. F., 2013, *MNRAS*, 436, 1096

Capraro I., Naletto G., Barbieri C., Occhipinti T., Verroi E., Zoccarato P., Paola A. D., 2009, in *Proceedings of Science: Quantum of Quasars workshop*.  
 Castor J. I., Nussbaumer H., 1972, *MNRAS*, 155, 293  
 Cavazzani S., Ortolani S., Barbieri C., 2012, *MNRAS*, 419, 2349  
 Davis J., Tango W. J., Booth A. J., ten Brummelaar T. A., Minard R. A., Owens S. M., 1999, *MNRAS*, 303, 773  
 Dravins D., 2007, *High Time Resolution Astrophysics*. Springer, New York  
 Dravins D., Germanà C., 2008, in Phelan D., Ryan O., Shearer A., eds, *The Universe At Sub-Second Timescales*. AIP, USA, p. 284  
 Dravins D., LeBohec S., 2007, *Proc. SPIE*, 6986, 698609  
 Dravins D., Lindegren L., Mezey E., Young A. T., 1997, *Publications of the Astronomical Society of the Pacific*, 109, 173  
 Dravins D., et al., 2005, Technical report, *QuantEYE: Quantum Optics Instrumentation for Astronomy*. European Southern Observatory OWL Instrument Concept Study  
 Dravins D., LeBohec S., Jensen H., Nuñez P. D., for the CTA Consortium 2013, *Astroparticle Physics*, 43, 331  
 Dravins D., Lagadec T., Nuñez P. D., 2015, *Nat. Commun.*, 6, 6852  
 Foellmi C., 2009, *A&A*, 507, 1719  
 Fox M., 2006, *Quantum Optics: An Introduction*. Oxford University Press, UK  
 Ghioni M., Armellini G., Maccagnani P., Rech I., Emsley M., Unlu M., 2008, *Photonics Technology Letters, IEEE*, 20, 413  
 Glauber R., 1963, *Phys. Rev.*, 131, 2766  
 Green J. M., 1980, *J. Phys. E: Sci. Instrum.*, 13, 1302  
 Hanbury-Brown R., 1974, *The Intensity Interferometer: Its Application To Astronomy*. Taylor & Francis ; Halsted Press, London ; New York  
 Hanbury-Brown R., Twiss R. Q., 1954, *Phil. Mag.*, 45, 663  
 Hanbury-Brown R., Twiss R. Q., 1956, *Nature*, 178, 1046  
 Hyland D., 2005, *Proc. SPIE*, 5905: Techniques and Instrumentation for Detection of Exoplanets II, 590511  
 Johansson S., Letokhov V. S., 2005, *New Astronomy*, 10, 361  
 Kral L., Prochazka I., Blazej J., Hamal K., 2004, *Proc. SPIE*, 5240  
 Kurtsiefer C., Zarda P., Mayer S., Weinfurter H., 2001, *J. Mod. Opt.*, 48(13), 2039  
 LeBohec S., et al., 2008, *Proc. SPIE*, 7013, 70132E  
 Lieu R., Hillman L. W., 2003, *ApJ*, 585, L77  
 Ling A., Peloso M. P., Marcikic I., Scarani V., Lamas-Linares A., Kurtsiefer C., 2008, *Phys. Rev. A*, 78, 020301  
 Loudon R., 2000, *The Quantum Theory of Light*. Oxford Science Publications  
 Mandel L., Wolf E., 1995, *Optical Coherence and Quantum Optics*. Cambridge University Press  
 Marini J. W., Murray C. W., 1973, Report X-591-73-35, Correction of laser range tracking data for atmospheric refraction at elevations above 10 degrees. NASA  
 Maziashvili M., 2009, *Astroparticle Physics*, 31, 344  
 Milburn G. J., 1991, *Phys. Rev A*, 44, 5401  
 Milburn G. J., 2006, *New J. Phys.*, 8  
 Millour F., 2008, *New Astronomy Reviews*, 52, 177  
 Millour F., 2010, *RevMexAA*, 38, 1  
 Morgan B. L., Mandel L., 1966, *Phys. Rev. Lett.*, 16, 1012  
 Ng Y. J., Christiansen W. A., van Dam H., 2003, *ApJ*, 591, L87  
 Nuñez P. D., 2012, *Towards Optical Intensity Interferometry For High Angular Resolution Stellar Astrophysics*. Department of Physics and Astronomy, University of Utah  
 Ofir A., Ribak E. N., 2006, *Proc. SPIE*, 6268, 165  
 Perlman E. S., Rappaport S. A., Christiansen W. A., Ng Y. J., DeVore J., Pooley D., 2015, *ApJ*, 805, 1  
 Ragazzoni R., Turatto M., Gaessler W., 2003, *ApJ*, 587, L1  
 Roche P. F., Colling M. D., Barlow M. J., 2012, *MNRAS*, 427, 581

- Saleh B. E. A., Teich M. C., 2007, *Fundamentals of Photonics*.  
John Wiley & Sons
- Stokes L. F., 1994, *IEEE Circuits and Devices Magazine*, 10, 46
- Strekalov D. V., Erkmen B. I., Yu N., 2013, *Phys. Rev A*, 88, 9
- Tan P. K., Yeo G. H., Poh H. S., Chan A. H., Kurtsiefer C., 2014,  
*ApJ*, 789, L10
- Varshni Y. P., Nasser R. M., 1986, *Astrophysics and Space Science*, 125, 341
- Woolf H. M., 1968, Technical report, On the computation of solar elevation angles and the determination of sunrise and sunset times. NASA technical memorandum X-1646
- van der Hucht K. A., 2001, *New Astronomy Reviews*, 45, 135

This paper has been typeset from a  $\text{\TeX}/\text{\LaTeX}$  file prepared by the author.